

Single photons emitted by nano-crystals optically trapped in a deep parabolic mirror

Vsevolod Salakhutdinov,^{1,2} Markus Sondermann,^{1,2,*} Luigi Carbone,³
Elisabeth Giacobino,^{4,2} Alberto Bramati,⁴ and Gerd Leuchs^{2,1,5}

¹*Friedrich-Alexander-Universität Erlangen-Nürnberg (FAU),*

Department of Physics, Staudtstr. 7/B2, 91058 Erlangen, Germany

²*Max Planck Institute for the Science of Light, Staudtstr. 2, 91058 Erlangen, Germany*

³*CNR NANOTEC-Institute of Nanotechnology c/o Campus Ecotekne,*

University of Salento, via Monteroni, Lecce 73100, Italy

⁴*Laboratoire Kastler Brossel, Sorbonne Université, CNRS,*

ENS-PSL, Research University, Collège de France,

4 place Jussieu, case 74 F-75005 Paris, France

⁵*Department of Physics, University of Ottawa, Ottawa, Ont. K1N 6N5, Canada*

We investigate the emission of single photons from CdSe/CdS dot-in-rods which are optically trapped in the focus of a deep parabolic mirror. Thanks to this mirror, we are able to image almost the full 4π emission pattern of nanometer-sized elementary dipoles and verify the alignment of the rods within the optical trap. From the motional dynamics of the emitters in the trap we infer that the single-photon emission occurs from clusters comprising several emitters. We demonstrate the optical trapping of rod-shaped quantum emitters in a configuration suitable for efficiently coupling an ensemble of linear dipoles with the electromagnetic field in free space.

a. Introduction Nano-scale light sources are used in many areas of research and applications. Examples range from the use of fluorescent nano-beads in microscopy to the role of various nanometer-sized solid-state systems as sources of single photons in future quantum technology applications. One approach to efficiently collect the emitted photons is to place the source at the focus of a parabolic mirror (PM) spanning a huge fraction of the full solid angle. Such a mirror has been used to study a laser cooled atomic ion held in a radio-frequency trap in vacuum [1]. More recently, the optical trapping of CdSe/CdS dot-in-rod particles in a deep PM in air has been demonstrated [2], and lately also the fabrication of a microscopic diamond PM around a nitrogen vacancy centre [3].

CdSe/CdS dot-in-rod (DR) particles have the remarkable properties of being single-photon emitters at room temperature as well as emitting light with a high degree of linear polarization [4]. The latter property stems from the fact that their emission is dominated by a linear-dipole transition [5]. In order to maximize the collection efficiency when using a PM, the axis of the linear dipole has to be aligned with the mirror's optical axis [6, 7]. Once this is achieved, a PM with the geometry used in Refs. [6, 7] as well as here collimates 94% of the emission of a linear dipole, exceeding the capabilities of a realistic lens-based set-up by a factor of two. Moreover, the same requirement has to be fulfilled when reversing this scenario, i.e. when focusing a linear-dipole mode with the purpose of exciting a single quantum emitter with high efficiency [6]. Any tilt of the quantization axis off the PM's axis will lead to a reduced field amplitude along the transition dipole moment of the target.

For CdSe/CdS DR particles, the dipole-moment of the excitonic transition is found to be aligned along

the c-axis of the rod [5, 8, 9]. Hence, the rod has to be aligned along the optical axis of the PM for maximizing the collection efficiency. This should occur in a natural way in an optical trap that is built by focusing a radially polarized beam as in Ref. [2]: The electric field in the focus of the PM is purely longitudinal, i.e. parallel to the PM axis. Since the polarizability of a rod is largest along its symmetry axis [10], the DR should thus be aligned along the optical axis of the PM. However, when trapping the particle under ambient conditions, this alignment is counteracted by random collisions with air molecules which exert a random torque on the DR (see, e.g. Refs. [11, 12]). Thus, the torque induced by the trapping laser onto the rod has to be larger than this random torque in order to achieve a good alignment of the rods.

The purpose of this work is two-fold: One aspect is checking the orientation of the DRs with respect to the optical axis of the PM. This is done by analyzing the spatially resolved pattern of the photons emitted by CdSe/CdS DR-particles. Since the rods' alignment is governed by their geometry and independent of the small CdSe core, our results should be applicable for many types of rod-shaped quantum emitters. In this sense, the CdSe/CdS DR-particles can be considered as a proof model. We again emphasize that a favorable alignment of a rod-shaped quantum-system is a mandatory prerequisite for efficient photon collection as well as for efficient excitation.

The other aspect treated here is specific to the CdSe/CdS DR-particles. We will show that clusters of DRs can act as a source of single photons. As a matter of fact, it will turn out that indeed all single-photon sources observed in our experiment are constituted by clusters of emitters. The emission of single photons from clusters of DRs demonstrated here is in good agreement with recent observations of the same phenomenon for CdSe/CdS core-shell dots [13].

b. Experimental procedure The CdS/CdSe DR-particles investigated here consist of a spherical CdSe core with 2.7 nm diameter. The core is embedded in a

* markus.sondermann@fau.de

CdS rod with a nominal length of 35 nm and diameter of 7 nm. Fluorescent photons are emitted at wavelengths about $\lambda_{\text{DR}} = 605$ nm. The DRs are trapped at ambient conditions in air at the focus of a deep parabolic mirror in an optical dipole-trap (see Ref. [2] and Fig. 3 in appendix for details). The electric field at wavelength $\lambda_{\text{trap}} = 1064$ nm in the focal region is polarized along the optical axis of the PM, which is here defined as the z -direction.

At the beginning of each experiment the power of the trapping laser is set to 360 mW and the pulsed excitation beam is switched off. Successful trapping of DR particles is witnessed by the onset of a fluorescence signal and from scattered trap light. The fluorescence is detected with a pair of avalanche photo-diodes (APDs). At this stage, fluorescence photons stem from two-photon excitation at λ_{trap} [2]. To determine the intensity auto-correlation function $g^{(2)}(t=0)$, the power of the trapping laser is reduced such that the count rate of photons on the APDs is hidden in the background noise. Then, more efficient pulsed excitation at $\lambda_{\text{exc}} = 405$ nm is switched on and the value of $g^{(2)}(t=0)$ is measured.

In case that $g^{(2)}(0) < 0.5$ is observed, i.e. the signature of single-photon emission, the experiment is continued as follows: Images of the spatial intensity distributions of fluorescence photons as found in the output aperture of the PM (see example in Fig. 2) are acquired with an electron-multiplying charge-coupled device (EMCCD) camera at several trapping beam powers. For each power setting we have averaged over several images, with an exposure time of 2 s per image. Vertically and horizontally polarized components are recorded simultaneously on different parts of the camera chip.

Next, the trapping beam power is set again to 360 mW and the motional dynamics of the particles in the trap is analyzed. The light scattered and Doppler-shifted by the particle interferes with the trapping light [14]. The corresponding interference signal is measured with a balanced detector (cf. Ref. [2]). From the time series of this signal we compute the power-spectral density which contains several Lorentzian-shaped features, each of which corresponds to the motion of the particle in the trap along a certain direction. The width Γ_i ($i = x, y, z$) of each of these peaks is proportional to the ratio r_i/m , where r_i is the radius of the trapped object and m its mass [15]. Since the particles used here are non-spherical, we interpret r_i as the radius of a disc that has the same area as the particle's surface when viewed from the direction of motion (see sketch in Fig. 1b). With m being proportional to the volume of the trapped object, Γ_i shrinks with increasing object size. Fitting a Lorentzian function to the power spectral density yields the axial damping rate Γ_z of the particles' motion [2]. The motion in radial direction is damped such strong that a corresponding spectral feature cannot be discerned.

Finally, the trapping beam power is gradually decreased to determine the power P_{min} at which the particle is lost from the trap. The loss of the trapped particles was monitored via the signal of the balanced

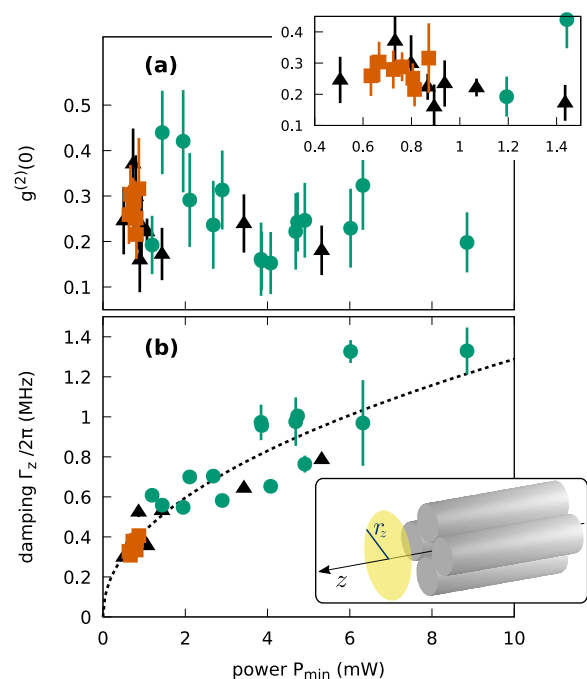


Figure 1. (a) Normalized second-order intensity correlation $g^{(2)}(0)$ of fluorescence photons emitted by DRs against power P_{min} at which the particles escaped the trap. Error bars show the Poissonian uncertainty. Green circles denote experiments in which the spatial intensity pattern revealed azimuthal symmetry and an obvious alignment of the rods to the axis of the PM. A single such data point with $P_{\text{min}} = 22$ mW and $g^{(2)}(0) = 0.19$ is off scale. Orange squares correspond to cases where the emission pattern shows a clear azimuthal asymmetry. Black triangles mark experiments with an inconclusive outcome. The inset shows a magnified view for low power levels. (b) Damping rate of axial motion Γ_z of trapped nano-particles against P_{min} . Error bars denote the 95% confidence interval of the fit from which Γ_z was obtained. The dashed line denotes the function $\Gamma_z \propto P_{\text{min}}^{0.48 \pm 0.03}$, with the power scaling obtained from a fit. The inset is a pictorial view of a cluster of rods aligned along the optical axis of the PM (z -axis). The yellow disc with radius r_z denotes the effective area of the cluster relevant for damping the motion along the z -axis.

detector.

c. Single-photon emission from clusters In our experiments, we observed $g^{(2)}(0) < 0.5$ for 33 different loads of the trap, see Fig. 1(a). The probability to trap a sample with this characteristic is approximately 10%. The observed values $0.15 \leq g^{(2)}(0) \leq 0.44$ agree well with the ones observed for single DRs with comparable geometry in literature [16, 17]. Therefore, one could conclude that the trapped objects are indeed single DRs. But this conclusion is contradicted by the observation that all trapped particles, which appear as single-photon emitters, are lost at powers in the range $0.5 \text{ mW} < P_{\text{min}} < 22 \text{ mW}$, with an average value of $2.5 \pm 2.1 \text{ mW}$, see histogram in Fig. 4 in the appendix. As derived there, the power at which the trapping potential for a single DR equals $k_B T$ at ambient temperature is $P_{\text{min}} \approx 41 \text{ mW}$. Therefore, a single DR that thermalizes to room temperature should be lost at about this power value. The vol-

ume and hence the polarizability of a trapped cluster consisting of several rods scales with the number of rods. The magnitude of P_{\min} consequently reduces by the same factor. Thus, one can infer that the smallest cluster displayed in Fig. 1 must contain at least four DRs and that the average number of rods in a cluster is 16 ± 14 .

It is also evident from the same figure that two branches in the scattered data points are apparent. In one of these regions, which extends towards power values $P_{\min} \lesssim 1.5$ mW, the data points are densely packed. We will refer to these samples as ‘large clusters’. At $P_{\min} > 1.5$ mW the data points are less dense. These samples will be called ‘small clusters’. The above threshold value of P_{\min} corresponds to approximately 27 rods. Further below we show that these two branches are linked to qualitative differences in the spatial intensity pattern of the emitted photons, influenced by the geometry of the clusters and their relative alignment to the PM axis. Independent of these differences, each branch has the property that $g^{(2)}(0)$ tends to increase with decreasing P_{\min} or increasing cluster size, respectively.

The trapping of clusters is furthermore confirmed by analyzing the damping rate of the particles’ motion inside the trap. Figure 1(b) shows the axial damping rate Γ_z as a function of P_{\min} . One observes a clear correlation of the two quantities with $\Gamma_z \propto \sqrt{P_{\min}}$. Since Γ_z increases with a decreasing size of the trapped object, we conclude that the variation in P_{\min} is due to the variation of the size and, therefore, to the polarizability of the trapped object. Furthermore, all observed damping rates are smaller than the one estimated for a single DR ($\Gamma_{\text{1DR}}/2\pi \geq 2$ MHz, see appendix). Hence, the trapped emitters of different size must be clusters consisting of differing numbers of DRs.

Surprisingly, the trapping of DRs in clusters occurs despite the use of toluene as working solvent that should suppress the formation of clusters in the aerosol sprayed in the trapping region. Possibly, clusters might form inside the optical trap as soon as several single DRs diffuse in the focal region of the PM.

The observation of pronounced antibunching in the emission from a cluster of sources proves the emission of single photons. This is not to be expected at first sight, however, but in good agreement with findings in other experiments. In Ref. [18] the quenching of the emission of CdSe/CdS core-shell quantum-dots by Förster energy-transfer to a MoSe₂ mono layer was demonstrated, which has earlier been also observed within assemblies of CdSe dots [19, 20]. In principle, such an exchange could also occur between several DRs in a cluster provided that the spectra of excitonic transitions of the DRs constituting the cluster overlap. Recently, single-photon emission from clusters of CdSe/CdS core-shell dots has been attributed to Auger annihilation of excitons in neighboring nanocrystals [13]. For DRs trapped sufficiently close to each other the same mechanism might be responsible for single-photon emission.

d. Analysis of the fluorescence pattern We now investigate the spatial intensity pattern of the pho-

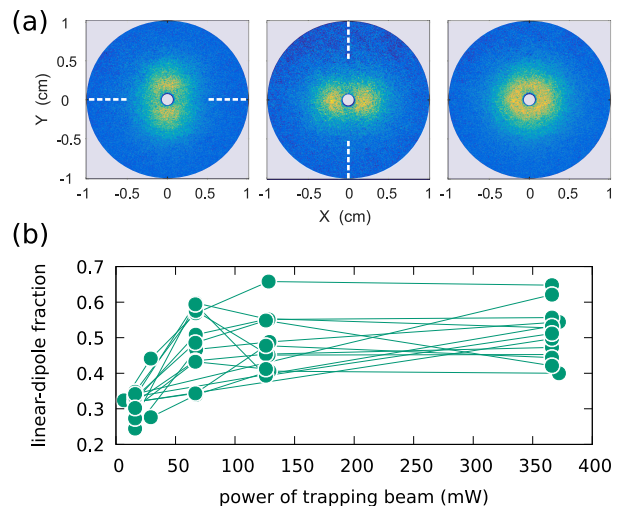


Figure 2. (a) Example of a spatial intensity pattern with rotational symmetry as observed in the aperture of the PM. The corresponding sample is the one with $P_{\min} = 2.9$ mW and $g^{(2)}(0) = 0.31$ in Fig. 1. From left to right the panels show the intensity when projected onto a vertical state of polarization, the projection onto a horizontal state of polarization, and the sum of the two, respectively. Dashed lines indicate the orientation of extinction lines as a guide to the eye. (b) Fraction of linear-dipole radiation in the fluorescence of small clusters of DRs as a function of trapping beam power. Values obtained in the same experimental run are connected by lines. The data points correspond to the ones depicted by circles in Figs. 1.

tons emitted by the DRs. Since the polarizability of a rod is larger along its symmetry axis than perpendicular to it, one expects that a single rod or a small enough cluster of parallel rods is oriented along the longitudinal electric field in the focus of the PM. Under this assumption and with the dipole moment of the exciton aligned along the rod, the intensity distribution of the photons collimated by the PM has to be symmetric under rotation around the optical axis of the PM. In the majority of loads (26 out of 33) the measured distribution of the total intensity exhibits this symmetry.

While a rotationally symmetric intensity pattern could in principle also be observed for an isotropic emitter, more insight can be gained from the polarization resolved emission pattern. For a linear dipole aligned parallel to the axis of the PM, the collimated emission is radially polarized [6]. After projection onto a linear state of polarization, the intensity distribution of a radially polarized state must exhibit extinction lines perpendicular to the projected polarization. This property is illustrated in the example displayed in Fig. 2(a). The observed extinction is not perfect, which is compatible with the existence of circular-dipole components in the DR emission.

The clusters which emit photons with a rotationally symmetric spatial distribution and which exhibit polarization patterns as described above are analyzed in further detail: We compute the azimuthal average of the total intensity distribution, resulting in a radial intensity profile [1]. Fitting a sum of the intensity dis-

tributions of linear and circular dipoles [21] to these profiles reveals the *measured* fraction of linear-dipole radiation (see App. D). This measured fraction will be lower than the one predicted by the properties of the excitonic transitions of the emitters due to the residual thermal vibration of the rods. The latter results in randomly fluctuating tilts of the rod off the PM's axis. With tilts into all directions being equally likely, a linear dipole appears not as a pure linear dipole but is masked by a circular-dipole component in the long-time average. However, the thermal vibrations are counteracted by the longitudinal electric field of the trap. This field exerts a torque onto non-aligned rods and re-orient them along the PM axis. Therefore, a stronger suppression of random tilts should occur at larger field amplitudes, i.e. at larger trapping beam powers. One thus expects to observe a larger linear-dipole fraction at larger trapping beam powers.

Indeed, 16 samples exhibit such a behavior, as is evident from Fig. 2(b). This confirms the alignment of the rods along the PM axis on average. Besides one exception, all samples (marked with circles in Figs. 1) showing axial alignment were lost from the trap at $P_{\min} > 1.5$ mW. These samples also constitute the group with the largest damping rates. Therefore, we conclude that the samples lost at $P_{\min} > 1.5$ mW are small clusters of DRs that are aligned along the axial trapping field. It should be noted that there is no correlation between the linear-dipole fraction measured at large trapping beam power and the power P_{\min} at which samples are lost from the trap. Alignment along the field of an optical trapping beam was previously observed also for silicon nanorods [12] and nanodiamonds [11, 22] as well as for nanorods trapped in a liquid [23, 24].

Most of the samples lost at low powers show no uniquely classifiable behavior in terms of emission pattern. This hints at emission from a large cluster without a pronounced structural order. Some of these large clusters show an emission pattern without rotational symmetry, i.e. with the dipole axis tilted off the PM's optical axis. We conjecture that these cases correspond to emission from DRs that are attached to a large main cluster under a non-zero angle. However, once released from the trap the clusters are inevitably lost, hindering a posteriori investigations of the clusters' structure.

A tempting explanation why the majority of aligned samples is found among the small clusters can be constructed from a geometric argument as follows: If the rods are aligned parallel to each other in closest packing, the width of the cluster equals the length of a single rod for a number of about 20 rods, resulting in an object of approximately equal size along all spatial dimensions and leading to the loss of pronounced directionality. In the experiments the apparent change

from the alignment of clusters along the PM axis to no preferential alignment occurs at a number of about 27 rods. This is in reasonable agreement with the number inferred just above. But the fact that some of the large clusters exhibit radiation patterns lacking rotational symmetry hints at a more complicated scenario.

Finally, it would be interesting to compare the measured count rates of photons emitted by the DRs to the ones expected for our set-up, in particular for the samples exhibiting alignment. However, a reliable quantitative comparison is hindered by the fact that the investigated samples exhibit blinking, as detailed in App. E.

e. Concluding discussion We have analyzed the fluorescence photons emitted by CdSe/CdS DRs which are optically trapped at the focus of a deep PM. The observation of single-photon emission from clusters of sources will be advantageous for applications, since clusters can be kept in the trap at trapping beam powers that are lower than necessary for single emitters. Moreover, for low trapping beam powers the excitation of the DRs via two-photon absorption [2] can be strongly suppressed, which promises a better timing accuracy for the emission of photons in a pulsed excitation scheme.

On the one hand, it could be possibly argued that the trapping of clusters of DRs, i.e. the fact that so far not a single isolated DR was trapped, might be detrimental to the efficient coupling of light to these emitters. On the other hand, this appears as a favorable condition to possibly promote the enhancement of the coupling due to collective effects when trapping a cluster of quantum targets. Also in cavity quantum-electrodynamics collective effects have been used advantageously [25–29]. There, large fractions of the ensemble can be hosted in the cavity mode [27, 28]. When coupling light and ensembles in free-space by tight focusing, the ensemble has to be located within the focal spot, which is of dimensions of the order of half a wavelength under optimum conditions [30, 31]. This is very difficult to achieve with ions due to Coulomb repulsion. Therefore, locating small clusters of optically trapped solid-state quantum targets in the focus of a linear-dipole wave is a feasible path towards combining tight focusing and ensemble physics.

ACKNOWLEDGMENTS

The authors thank M. Manceau for fruitful discussions. G.L. acknowledges financial support from the European Research Council (ERC) via the Advanced Grant 'PACART'.

-
- [1] R. Maiwald, A. Golla, M. Fischer, M. Bader, S. Heugel, B. Chalopin, M. Sondermann, and G. Leuchs, *Phys. Rev. A* **86**, 043431 (2012).
 [2] V. Salakhutdinov, M. Sondermann, L. Carbone,

- E. Giacobino, A. Bramati, and G. Leuchs, *Optica* **3**, 1181 (2016).
 [3] N. H. Wan, B. J. Shields, D. Kim, S. Mouradian, B. Lienhard, M. Walsh, H. Bakhru, T. Schröder, and

- D. Englund, *Nano Letters* **18**, 2787 (2018).
- [4] F. Pisanello, L. Martiradonna, G. Leménager, P. Spinicelli, A. Fiore, L. Manna, J.-P. Hermier, R. Cingolani, E. Giacobino, M. D. Vittorio, and A. Bramati, *Applied Physics Letters* **96**, 033101 (2010).
- [5] S. Vezzoli, M. Manceau, G. Leménager, Q. Glorieux, E. Giacobino, L. Carbone, M. De Vittorio, and A. Bramati, *ACS Nano* **9**, 7992 (2015).
- [6] N. Lindlein, R. Maiwald, H. Konermann, M. Sondermann, U. Peschel, and G. Leuchs, *Laser Physics* **17**, 927 (2007).
- [7] M. Sondermann and G. Leuchs, in *Engineering the Atom-Photon Interaction: Controlling Fundamental Processes with Photons, Atoms and Solids*, Nano-Optics and Nanophotonics, edited by A. Predojević and M. W. Mitchell (Springer International Publishing, 2015) pp. 75–98, arXiv:1411.7287.
- [8] A. L. Efros, M. Rosen, M. Kuno, M. Nirmal, D. J. Norris, and M. Bawendi, *Phys. Rev. B* **54**, 4843 (1996).
- [9] M. Manceau, *Single CdSe/CdS dot-in-rods fluorescence properties*, Ph.D. thesis, Université Pierre et Marie Curie-Paris VI (2014).
- [10] B. A. Stickler, S. Nimmrichter, L. Martinetz, S. Kuhn, M. Arndt, and K. Hornberger, *Physical Review A* **94**, 033818 (2016).
- [11] T. M. Hoang, Y. Ma, J. Ahn, J. Bang, F. Robicheaux, Z.-Q. Yin, and T. Li, *Physical Review Letters* **117**, 123604 (2016).
- [12] S. Kuhn, A. Kosloff, B. A. Stickler, F. Patolsky, K. Hornberger, M. Arndt, and J. Millen, *Optica* **4**, 356 (2017).
- [13] B. Lv, H. Zhang, L. Wang, C. Zhang, X. Wang, J. Zhang, and M. Xiao, *Nature Communications* **9**, 1536 (2018).
- [14] P. Mestres, J. Berthelot, M. Spasenović, J. Gieseler, L. Novotny, and R. Quidant, *Applied Physics Letters* **107**, 151102 (2015).
- [15] L. P. Neukirch and A. N. Vamivakas, *Contemporary Physics* **56**, 48 (2015).
- [16] S. Vezzoli, S. Shojaii, S. Cialdi, D. Cipriani, F. Castelli, M. G. Paris, L. Carbone, P. D. Cozzoli, E. Giacobino, and A. Bramati, *Optics Communications* **300**, 215 (2013).
- [17] M. Manceau, S. Vezzoli, Q. Glorieux, F. Pisanello, E. Giacobino, L. Carbone, M. De Vittorio, and A. Bramati, *Phys. Rev. B* **90**, 035311 (2014).
- [18] K. M. Goodfellow, C. Chakraborty, K. Sowers, P. Waduge, M. Wanunu, T. Krauss, K. Driscoll, and A. N. Vamivakas, *Applied Physics Letters* **108**, 021101 (2016).
- [19] C. R. Kagan, C. B. Murray, M. Nirmal, and M. G. Bawendi, *Phys. Rev. Lett.* **76**, 1517 (1996).
- [20] S. A. Crooker, J. A. Hollingsworth, S. Tretiak, and V. I. Klimov, *Phys. Rev. Lett.* **89**, 186802 (2002).
- [21] M. Sondermann, N. Lindlein, and G. Leuchs, arXiv:0811.2098 (2008), 0811.2098v3.
- [22] M. Geiselmann, M. L. Juan, J. Renger, J. M. Say, L. J. Brown, F. J. G. de Abajo, F. Koppens, and R. Quidant, *Nature Nanotechnology* **8**, 175 (2013).
- [23] P. V. Ruijgrok, N. R. Verhart, P. Zijlstra, A. L. Tchebotareva, and M. Orrit, *Phys. Rev. Lett.* **107**, 037401 (2011).
- [24] C. R. Head, E. Kammann, M. Zanella, L. Manna, and P. G. Lagoudakis, *Nanoscale* **4**, 3693 (2012).
- [25] R. J. Thompson, G. Rempe, and H. J. Kimble, *Phys. Rev. Lett.* **68**, 1132 (1992).
- [26] A. Lambrecht, T. Coudreau, A. M. Steinberg, and E. Giacobino, *EPL (Europhysics Letters)* **36**, 93 (1996).
- [27] F. Brennecke, T. Donner, S. Ritter, T. Bourdel, M. Köhl, and T. Esslinger, *Nature* **450**, 268 (2007).
- [28] Y. Colombe, T. Steinmetz, G. Dubois, F. Linke, D. Hunger, and J. Reichel, *Nature* **450**, 272 (2007).
- [29] P. F. Herskind, A. Dantan, J. P. Marler, M. Albert, and M. Drewsen, *Nature Physics* **5**, 494 (2009).
- [30] I. Gonoskov, A. Aiello, S. Heugel, and G. Leuchs, *Phys. Rev. A* **86**, 053836 (2012).
- [31] L. Alber, M. Fischer, M. Bader, K. Mantel, M. Sondermann, and G. Leuchs, *Journal of the European Optical Society-Rapid Publications* **13**, 14 (2017), arXiv:1609.06884.
- [32] R. J. Lang, *The Journal of the Acoustical Society of America* **34**, 6 (1962).
- [33] F. Barreras, H. Amaveda, and A. Lozano, *Experiments in Fluids* **33**, 405 (2002).
- [34] L. Carbone, C. Nobile, M. De Giorgi, F. D. Sala, G. Morello, P. Pompa, M. Hytch, E. Snoeck, A. Fiore, I. R. Franchini, M. Nadasan, A. F. Silvestre, L. Chiodo, S. Kudera, R. Cingolani, R. Krahne, and L. Manna, *Nano Letters* **7**, 2942 (2007).
- [35] P. Spinicelli, S. Buil, X. Quélin, B. Mahler, B. Dubertret, and J.-P. Hermier, *Phys. Rev. Lett.* **102**, 136801 (2009).
- [36] F. Pisanello, G. Leménager, L. Martiradonna, L. Carbone, S. Vezzoli, P. Desfonds, P. D. Cozzoli, J.-P. Hermier, E. Giacobino, R. Cingolani, M. De Vittorio, and A. Bramati, *Advanced Materials* **25**, 1974 (2013).
- [37] C. Galland, Y. Ghosh, A. Steinbrück, M. Sykora, J. A. Hollingsworth, V. I. Klimov, and H. Htoon, *Nature* **479**, 203 (2011).
- [38] D. C. Moore, A. D. Rider, and G. Gratta, *Phys. Rev. Lett.* **113**, 251801 (2014).
- [39] M. Frimmer, K. Luszcz, S. Ferreira, V. Jain, E. Hebestreit, and L. Novotny, *Phys. Rev. A* **95**, 061801(R) (2017).

Appendix A: Experimental set-up

Figure 3 shows a schematic of the experimental set-up. Nano-particles are trapped at ambient conditions in air at the focus of a deep parabolic mirror (PM). The PM has a focal length of 2.1 mm and an aperture radius of 10 mm, which corresponds to a half-opening angle of 134° . A bore hole with 1.5 mm diameter at the vertex of the PM allows for the delivery and the optical excitation of the nanoparticles. Based on these geometrical boundary conditions the collection efficiency for photons in a linear-dipole mode (circular-dipole mode) cannot exceed 94% (76%), where the quantization axis is defined to coincide with the optical axis of the PM. The reflectivity of the PM was determined to be 72%.

The trapping beam is radially polarized and has the intensity pattern of a Laguerre-Gaussian mode of first radial order ('doughnut mode'). The electric field at wavelength $\lambda_{\text{trap}} = 1064 \text{ nm}$ in the focal region is polarized along the optical axis of the PM, which is here defined as the z -direction.

The CdS/CdSe dot-in-rod (DR) particles are surrounded by alkyl chains stored in toluene, hindering the clustering of particles. We use a home-built, toluene-resistant nebulizer for delivering DR particles to the trapping region through an opening at the vertex of the PM. The nebulizer comprises a piezo-electric transducer that is driven with an alternating voltage oscillating at about 360 – 390 kHz. For these frequencies one expects an aerosol of toluene droplets with a mean diameter of $6 \mu\text{m}$ [32, 33]. The nebulizer is filled with toluene containing DR particles in concentrations ranging from 6×10^4 to 6×10^8 DRs/l. We thus expect less than 10^{-4} DRs in a single droplet of about 100 fl volume on average.

Light scattered and Doppler-shifted by the particle interferes with the trapping light [14]. The corresponding interference signal is measured with a balanced detector (cf. Fig. 3 and Ref. [2]). The balancing is achieved with light that is tapped off the trap laser beam and adjusted in amplitude by a neutral-density filter (NDF).

Trapped DR particles are optically excited at a wavelength $\lambda_{\text{exc}} = 405 \text{ nm}$ with pulses of 82 ns duration and $2 \mu\text{W}$ average power. The pulse repetition rate is 10^6 s^{-1} . The excitation pulse power is chosen such that the DRs are approximately saturated, i.e. on average one exciton is created per excitation pulse [16]. The DRs emit photons at wavelengths about $\lambda_{\text{DR}} = 605 \text{ nm}$, which are picked off the excitation and trapping beam path by a reflective short-pass filter that attenuates light at λ_{trap} in reflection. The fluorescence photons are analyzed by either a pair of APDs with 69% quantum efficiency for determining the second-order intensity correlation function $g^{(2)}(t)$ or by an EMCCD camera for measuring the spatial intensity distribution as found in the output aperture of the PM. This aperture is imaged onto the camera by a demagnifying telescope. Vertically and horizontally polarized components are split by a polarizing beam splitter (PBS) and recorded simultaneously on different parts of the camera chip. The APDs as well as the camera are equipped with band-pass filters which reject light at λ_{exc} and at λ_{trap} . Not accounting for the reflectivity of the PM as well as the APDs' quantum efficiency, the transmission of the set-up was measured to be 83%.

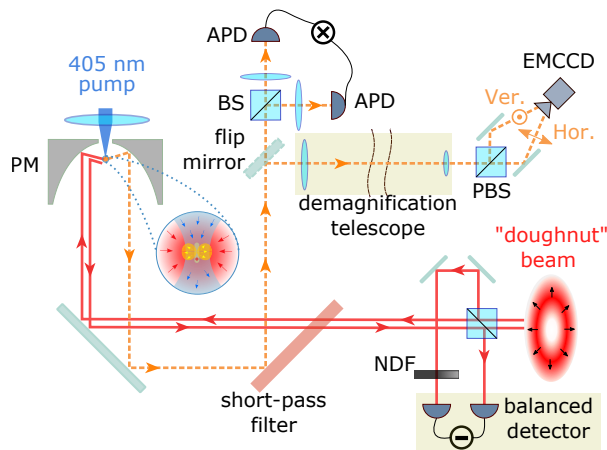


Figure 3. Scheme of the experimental set-up. CdSe/CdS dot-in-rod (DR) particles are trapped in an optical tweezers by focusing a radially polarized infrared laser beam ('doughnut beam') with a parabolic mirror (PM). The DRs are optically excited by a blue pulsed laser ('pump'). Fluorescent photons are collimated by the PM and either detected by two avalanche photo-diodes (APDs), which are separated by a beam splitter (BS), or an electron-multiplying charge-coupled device (EMCCD) camera. A polarizing beam splitter (PBS) in front of the EMCCD camera projects the photons onto horizontally and vertically polarized states measured by different sections of the camera chip. The motion of the DRs is characterized by detection of the light of the trap laser that is scattered by the DRs and interferes with trap light back-reflected by the PM. This signal is balanced with light that is tapped off the trap laser beam and adjusted in amplitude by a neutral-density filter (NDF).

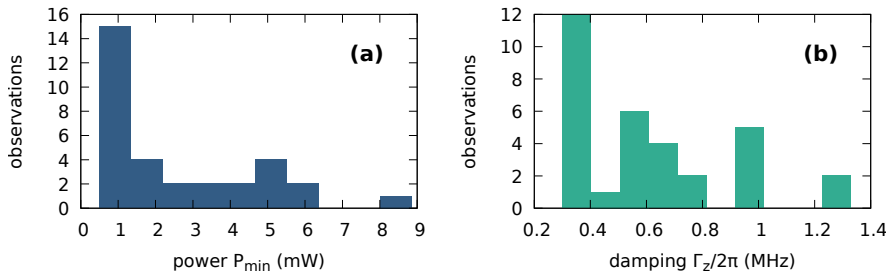


Figure 4. (a) Distribution of minimum trapping beam powers P_{\min} at which samples escaped the trap. (b) Distribution of damping rates Γ_z of the axial motion of the samples trapped in the experiment. The histograms have been computed for the data shown in Fig. 1 in the main text.

Appendix B: Minimum trapping beam power

The depth of the trapping potential of a dielectric particle in the Rayleigh approximation is given by $U_0 = \alpha/2 \cdot E_{\max}^2$, where α is the polarizability of the particle and E_{\max} is the maximum amplitude of the electric field in the focal region. E_{\max}^2 is proportional to the power of the focused trapping beam. The derivation of E_{\max} for our particular set-up can be found in Ref. [2]. Taking the polarizability α to be the one of a CdS rod aligned to the electric field, one has [12]

$$\alpha = \epsilon_0 V_{\text{rod}} (n_{\text{CdS}}^2 - 1) \quad (\text{B1})$$

with $n_{\text{CdS}} = 2.34$ the refractive index of CdS at λ_{trap} and V_{rod} the volume of the rod. Setting $U_0 = k_{\text{B}}T$ with $T = 296$ K yields $P_{\min} = 41$ mW.

The distribution of powers P_{\min} at which samples with $g^{(2)}(0) < 0.5$ escaped the trap is shown in Fig. 4. The average value (standard deviation) is 2.5(2.1) mW. This corresponds to an average number of 16(14) rods in a trapped cluster.

Appendix C: Damping of axial motion

For a spherical particle in air, the damping of its oscillatory motion is given by [15]

$$\Gamma = \frac{6\pi\eta r}{m} \cdot \frac{0.619}{0.619 + \text{Kn}} (1 + c_{\text{K}}) \quad , \quad (\text{C1})$$

with η the viscosity of air, r the sphere's radius and m its mass. $\text{Kn} = \Lambda/r$ is the Knudsen number with Λ the mean free-path length of an air molecule and $c_{\text{K}} = 0.31\text{Kn}/(0.785 + 1.152\text{Kn} + \text{Kn}^2)$.

Here, we interpret r as the radius of the area of the particle's surface as seen along the direction of motion. Hence, for a rod aligned parallel to the optical axis of the PM r is identified with the radius of the rod. Due to the attached alkyl chains, which have a length of about 1.6 nm, the *effective* radius of the rod is increased, resulting in $\Gamma_{\text{IDR}}/2\pi \approx 2$ MHz. Furthermore, due to residual vibration the trapped particles' effective radius is enlarged when averaging over the time constants of translational motion. The distribution of damping rates observed in the experiments for samples with $g^{(2)}(0) < 0.5$ is shown in Fig. 4. The average value (standard deviation) of $\Gamma_z/2\pi$ is 0.62(0.29) MHz.

Appendix D: Dipole radiation patterns

The analysis of the spatial intensity pattern of the photons emitted by the DRs is based on determining the relative fraction of linear- and circular-dipole radiation. We choose the quantization axis to coincide with the optical axis of the PM. Then, upon collimation by the PM the intensity distribution of a linear dipole reads [6, 21]

$$I_{\pi}(R) = I_{0,\pi} \cdot \frac{R^2}{(R^2/4 + 1)^4} \quad (\text{D1})$$

with $I_{0,\pi}$ a proportionality constant and R the radial distance to the optical axis of the PM in units of the mirror's focal length. The corresponding expression for a circular dipole reads

$$I_{\sigma}(R) = I_{0,\sigma} \cdot \frac{R^4/16 + 1}{(R^2/4 + 1)^4} \quad . \quad (\text{D2})$$

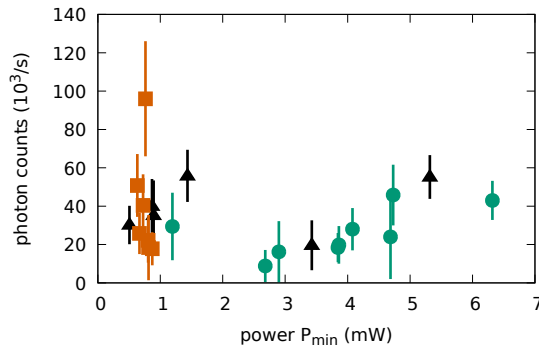


Figure 5. Photon count rates of trapped clusters as a function of power P_{\min} at which samples escaped the trap. The count rates correspond to the average rate of a grey state obtained by fitting a gaussian distribution to count rate histograms. The errorbars represent the rms width of the gaussian distribution. The meaning of different symbols is the same as in Fig. 1 in the main text.

The sum of these two distributions is fit to radial intensity profiles which are obtained by computing the azimuthal average of the images acquired with the EMCCD camera. The resulting fraction of linear-dipole radiation is then given by

$$A_{\pi} = \frac{I_{0,\pi}}{I_{0,\pi} + I_{0,\sigma}} \quad . \quad (\text{D3})$$

Appendix E: Photon count rates

In what follows, we first derive the photon count rate expected for the CdSe/CdS DRs and then compare to the ones observed in the experiment. One has to account for several characteristics of the investigated emitters. The number of electron-hole pairs created upon optical excitation with power P is given by P/P_{sat} , where P_{sat} is the saturation power defined as the power at which one exciton-hole pair is created on average [16]. The number of emitted photons is proportional to $(1 - \exp(-P/P_{\text{sat}}))$. We have determined P_{sat} from saturation measurements [16] using large ensembles of rods, i.e. clusters with intensity correlation $g^{(2)}(0) \approx 1$. The resulting value is $P_{\text{sat}} = 2.63 \pm 0.43 \mu\text{W}$. The used excitation power in all our experiments was $P = 2 \mu\text{W}$. Furthermore, the DRs have a non-unit quantum yield. The latter was previously determined to be about $Q_{\text{DR}} = 0.7$ [34].

In the experiment the photons are collected upon pulsed excitation from the auxiliary laser at a rate $\gamma_{\text{exc}} = 10^6/\text{s}$ and at strongly reduced trapping beam power. The latter condition results in an ineffective suppression of rod vibrations, such that the *measured* radiation pattern contains a fraction of linear-dipole radiation of $A_{\pi} = 0.31 \pm 0.03$ (cf. Fig. 2 in main text). The collection efficiency of the used PM itself is 94% for a linear dipole and 76% for circular dipole radiation.

Taking into account the APD's quantum efficiency Q_{APD} , the reflectivity R_{PM} of the PM, and the transmission T through the setup (all specified in Sec. A), the expected photon count rate is

$$\gamma_{\text{exc}} \cdot Q_{\text{APD}} \cdot T \cdot R_{\text{PM}} \cdot [1 - \exp(-P/P_{\text{sat}})] \cdot Q_{\text{DR}} \cdot [0.94 \times A_{\pi} + 0.76 \times (1 - A_{\pi})] = (125 \pm 14) \times 10^3 \text{ s}^{-1} \quad . \quad (\text{E1})$$

All samples investigated in the experiment show a blinking behavior which is well-known in literature. Therefore, for the analysis of the photon detection events we apply established methods accounting for this effect [17, 35, 36]. The time-resolved count rate of detected photons is obtained by binning the time-tagged detection events into a continuous series of intervals with a constant width of $500 \mu\text{s}$. From the resulting time series the distribution of count rates is computed. For some samples, the time series is dominated by intermittent bursts from a low light level. The corresponding histograms show an exponentially decaying distribution of count rates. For 22 samples the distribution of count rates exhibits a pronounced local maximum at nonzero detection rates. The average count rates corresponding to this local maximum are reported in Fig. 5. The observed rates are considerably below the expected rate.

However, the observed count rates are strongly fluctuating from sample to sample. The size of the cluster, i.e. the value of P_{\min} has no obvious influence onto the rate of detected photons. One might argue that there is a slight tendency of increasing count rate for increasing P_{\min} evident from Fig. 5 for small clusters with $P_{\min} > 1.5 \text{ mW}$, i.e. the aligned samples. But the corresponding count rates are of comparable magnitude to the rates observed for the large samples. Furthermore, the photon emission properties of all samples are investigated at low trapping beam powers, at which the alignment of the small clusters is weakest anyhow. There is also no evident correlation of count rate and the value of $g^{(2)}(0)$ (data not shown).

These observations indicate that the photon count rates are related to the photo-physics of the DRs and not the properties of the setup or the geometry of the trapped clusters. Furthermore, the blinking behaviour is typically characterized by distributions exhibiting two pronounced maxima at nonzero count rates (cf. e.g. Refs. [17, 35]), where the larger rate corresponds to a so-called ‘bright-state’ and the lower one to a so-called ‘grey state’ which is related to the presence of excess charges [37]. None of the samples investigated here exhibits two pronounced states. Due to the low photon count rates we associate the rates given in Fig. 5 with a grey state. In addition, the emission from a grey state is typically a factor 2 to 6 weaker than from a bright state [17, 35]. When applying this correction factor, many samples would exhibit an extrapolated bright state with count rates in reasonable agreement with the expected one. We attribute the dominance of emission from a grey state to particularly strong charging of the optically trapped samples. A potential origin of the charging is the process of spraying the aerosol containing the nano-particles into the trapping region. For example, also silica nano-spheres are typically charged after spraying [38, 39].